Applied Catalysis B: Environmental 217 (2017) 115–124

Contents lists available at ScienceDirect

Applied Catalysis B: Environmental

journal homepage: www.elsevier.com/locate/apcatb

# Heterostructured Ni/NiO composite as a robust catalyst for the hydrogenation of levulinic acid to γ-valerolactone

Song Song[a], Sikai Yao[a], Jiahui Cao[a], Lu Di[a], Guangjun Wu[a], Naijia Guan[a,b], Landong Li[a,b,*]

[a] School of Materials Science and Engineering & National Institute for Advanced Materials, Nankai University, Tianjin, 300350, PR China
[b] Key Laboratory of Advanced Energy Materials Chemistry of Ministry of Education, Collaborative Innovation Center of Chemical Science and Engineering, Nankai University, Tianjin, 300071, PR China

ARTICLE INFO

*Article history:*
Received 21 February 2017
Received in revised form 28 April 2017
Accepted 25 May 2017
Available online 30 May 2017

*Keywords:*
Ni/NiO
Heterojunctions
Hydrogenation
Levulinic acid
γ-Valerolactone

ABSTRACT

A non-precious metal catalyst Ni/NiO is developed for the efficient hydrogenation of levulinic acid to γ-valerolactone under mild conditions. Treating nickel oxide in hydrogen at controlled temperature of 473–573 K results in its partial reduction to metallic nickel and the formation of Ni/NiO heterojunctions, as indicated by the characterization results from in situ XRD, XPS and TEM. The as-prepared Ni/NiO catalyst exhibits remarkable activity in levulinic acid hydrogenation with a high mass activity of 14.1 mmol/h/g at 393 K, being over 18 times higher than NiO and 10 times higher than metallic Ni. Besides, Ni/NiO shows very good stability and recyclability during the reaction, making it a promising catalyst for practical levulinic acid hydrogenation. The formation of Ni/NiO heterojunctions is crucial for the remarkable activity of Ni/NiO composite catalyst and a cooperative Langmuir-Hinshelwood mechanism is proposed for levulinic acid hydrogenation on the basis of kinetic analysis and theoretical calculations. The concept of cooperative catalysis on metal/oxide heterojunctions can be expanded to other hydrogenation reactions.


## 1. Introduction

With increasing demands for chemicals and fuels, it is urgently desired to find sustainable alternatives for petroleum-based products [1,2]. Biomass, as a renewable carbon source coming from photosynthesis, attracts significant attention in the past decades. Lignocellulosic biomass, a key part of biomass, can be converted into valuable platform molecules, such as furfural [3,4], 5-hydromethylfurfura [5–13], levulinic acid [14], γ-valerolactone (GVL) [15,16], glycerol [17–19] and sorbitol [20], which can be further transformed into valuable chemicals and fuels. A major challenge in lignocellulosic biomass valorization is developing adequate catalysts to produce chemicals or fuels with high activity and selectivity [21]. Besides, for economic considerations, the use of non-precious metal-based catalysts instead of common precious metal catalysts for biomass valorization receives special interest [22–25].

GVL, an important biomass-derived renewable product, can be used as green solvent [26], an intermediate in fine chemicals synthesis [27,28] and also a flavoring agent [29]. There exists many pathways for GVL production [30–32], and the direct hydrogenation of levulinic acid to GVL shows significant economic advantages due to its low capital cost and energy consumption. Various transition metal catalysts have been employed for the direct hydrogenation of levulinic acid to GVL with hydrogen [33–39]. The catalytic activity of metal catalysts in the reaction is reported to follow the order of Ru > Ir > Rh > Pd > Pt > Re > Ni, and good GVL yields can be achieved with precious metal catalysts [30]. However, the high cost and scarcity of precious metals restrict their practical application. In contrast, non-precious metals, e.g. iron, cobalt and nickel, based catalysts often show lower activity and relatively higher temperatures are required to obtain good GVL yields [40–53]. Therefore, it is highly desired to go in-depth understanding of the catalytic active sites for a rational design of high-efficient non-precious metal catalysts.

Recently, Beller et al. reported the facile synthesis of non-precious metal (iron, cobalt and nickel) hydrogenation catalysts derived from the pyrolysis of phenanthroline metal acetate on solid support [54–56]. In case of cobalt catalysts, the catalytic active sites were attributed to metallic cobalt species with surface CoOx [55]. While Corma et al. proposed that the metallic cobalt species in the Co@C nanoparticles were the active phase for the chemose-

* Corresponding author at: School of Materials Science and Engineering & National Institute for Advanced Materials, Nankai University, Tianjin, 300350, PR China.
*E-mail address:* lild@nankai.edu.cn (L. Li).

http://dx.doi.org/10.1016/j.apcatb.2017.05.073
0926-3373/

lective hydrogenation of nitroarenes [57]. For the hydrogenation of levulinic acid to GVL, Han et al. reported that metallic cobalt species played an important role in the reaction [58]. In contrast to the debates on the hydrogenation sites in cobalt catalysts, metallic nickel species were generally regarded as the active sites in traditional nickel hydrogenation catalysts, which were not active at low reaction temperatures [30].

Herein, we report a simple and scalable strategy to high-efficient nickel hydrogenation catalyst, i.e. heterostructured Ni/NiO composite. High activity and perfect selectivity are achieved in the hydrogenation of levulinic acid to GVL over the as-prepared Ni/NiO, comparable with benchmark ruthenium catalyst under mild conditions. The combination of spectral characterizations, kinetic analysis and theoretical calculations reveal that the high hydrogenation activity is related with the formation of Ni/NiO heterojunctions from the partial reduction of nickel oxide.

## 2. Experimental

### 2.1. Catalyst preparation

The parent nickel oxide, i.e. NiO, was prepared via a chemical precipitation route. In a typical process, soluble nickel salt (nickel nitrate, nickel chloride, nickel sulfate or nickel acetate) was dissolved in 200 mL distilled water and the precipitator (1 M $Na_2CO_3$ solution) was added drop-wise into the nickel-containing aqueous solution under vigorous stirring until the pH of the mother liquid reaching about nine. The suspension was aged at 333 K for 8 h under stirring and the precipitate was collected by filtration, followed by thorough wash with distilled water. The solid product was dried at 353 K overnight and then calcined in the air at 673 K for 5 h to derive NiO.

The as-prepared NiO was further treated in pure hydrogen (flow rate = 20 mL/min) at designated temperature (473–773 K) for 1 h and the obtained products were labelled as NiO-K, where K indicated the treatment temperature in Kelvin.

### 2.2. Characterization techniques

The specific surface areas of samples were determined by $N_2$ adsorption/desorption isotherms at 77 K collected on a Quantachrome iQ-MP gas adsorption analyzer.

Transmission electron microscopy (TEM) images of selected samples were taken on a FEI Tecnai G2 F30 electron microscope at an acceleration voltage of 200 kV. A few drops of alcohol suspension containing the sample were placed on a carbon-coated copper grid, followed by evaporation at ambient temperature.

The temperature-programmed reduction (TPR) experiments of selected samples were performed on a chemisorption analyzer (Chemisorb 2720, Micromeritics) with 5 vol% $H_2$/Ar in the temperature range of 323–973 K at a heating rate of 10 K/min. Prior to reduction, the sample was pretreated in Ar at 523 K for 1 h.

The X-ray diffraction (XRD) patterns of NiO during in situ reduction process (473–773 K) were recorded on a Thermo ARL SCINTAG X'TRA diffractometer with Anton Parr XRK 900 reaction chamber using Cu-Kα radiation (λ = 0.1541 nm) at a scanning rate of 4°/min in the region of 2θ = 10–80°. The sample chamber atmosphere was maintained under flowing hydrogen at a flow rate of 20 mL/min.

X-ray photoelectron spectra (XPS) were recorded on a Thermo Scientific ESCALAB 250Xi spectrometer using monochromatic Al-Kα X-ray source (hν = 1486.6 eV) as the excitation source. NiO sample was in situ reduced in the reaction chamber, evacuated and transferred for analysis under vacuum. All spectra were recorded by using an aperture slot of 300 × 700 μm. Accurate binding energies (±0.1 eV) were determined with respect to the position of the adventitious C 1s peak at 284.8 eV.

FTIR spectra with CO as a probe were collected using a Bruker Tensor 27 spectrometer with 128 scans at a resolution of 2 $cm^{-1}$. A self-supporting pellet made of sample was placed in the reaction chamber and pretreated in flowing He at 573 K for 1 h. After cooling to room temperature in flowing He, the He stream was switched to 1% CO/He and a series of time-dependent FTIR spectra were sequentially recorded.

### 2.3. Catalytic study

The hydrogenation of levulinic acid was performed in a high-pressure stainless autoclave (Xinyuan Chemical Machinery, Series CJK, 300 mL) at a stirring rate of 750 rpm (adequate to exclude the external mass transfer limitation). In a typical experiment, 0.2 g catalyst, 10 mmol levulinic acid and 100 mL dioxane solvent were well mixed in the autoclave and purged with pure helium for five times at room temperature. The autoclave was rapidly heated to desired temperature and then hydrogen was introduced, typical at 2 MPa, to initiate the reaction.

After reaction, the liquid organic products were analyzed by gas chromatography (Shimadzu GC-2010) and gas chromatography–mass spectrometry (Shimadzu GCMS-QP2010 SE), both with a RXI-5MS column (30 m, 0.25 mm i.d., stationary phase thickness of 0.25 μm). *n*-Dodecane was used as an internal standard for quantification. The possible gas products were analyzed with a mass spectrometer (Pfeiffer Omnistar GSD 320).

### 2.4. Theoretical simulations

Spin polarized DFT calculations were preformed using the Vienna ab initio simulation package (VASP) [59,60], with the projector augmented wave (PAW) potentials [61]. The exchange-correlation functional with the generalized gradient approximation of Perdew, Burke and Eenzerh (GGA-PBE) [62] together with the Hubbard-U method [63] applied for the d-electrons of Ni atoms, which is referred to as PBE + U, was employed. The parameters describing the on-site Coulomb repulsion between the Ni 3d orbitals were chosen as U = 6.3 eV and J = 1 eV, which is adopted from previous studies [64–66]. A ferromagnetic (FM) and an antiferromagnetic (AFM) phase was adopted for Ni (111) and NiO (111), respectively. The electron wave function was expanded using plane waves with an energy cutoff of 400 eV.

For the calculation of hydrogen and hydrogen atom adsorption energy, a 3 × 3 × 1 k-point mesh was used and geometries were relaxed using the conjugate gradient algorithm until the forces on all unconstrained atoms were less than 0.01 eV/Å. The Ni (111) surface was represented by a four-layer slab and a p (2 × 2) supercell. The NiO (111) surface was modeled by a slab with four NiO double layers and the results were validated by using models with more layers. The p (2 × 2) O-terminated octopolar NiO (111) reconstruction with 3/4ML O missing at the top layer and 1/4 ML Ni missing at the second layer [67,68] was utilized in our study. The bottom two layers was constrained and a vacuum spacing greater than 10 Å was used in both two models.

Surfaces were constructed using 4 × 4 unit cells with four layers for the calculation of levulinic acid adsorption energy and the bottom two layers were fixed. The unit cell was sampled with the Γ point only. Structures were relaxed until the Hellmann-Feynman forces acting on the atoms were smaller than 0.05 eV/Å. The adsorption energy is defined as $E_{ads} = E_{surf+adsorbate} - E_{surf} - E_{adsorbate}$, where $E_{surf+adsorbate}$, $E_{surf}$ and $E_{adsorbate}$ are the calculated total energy of the surface with adsorbate, the surface, and the adsorbate species in the gas phase, respectively.

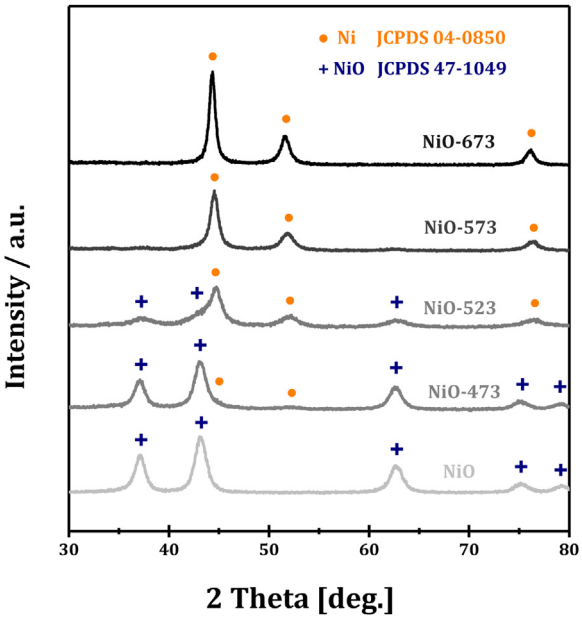


**Fig. 1.** In situ XRD patterns of NiO reduced at different temperatures.

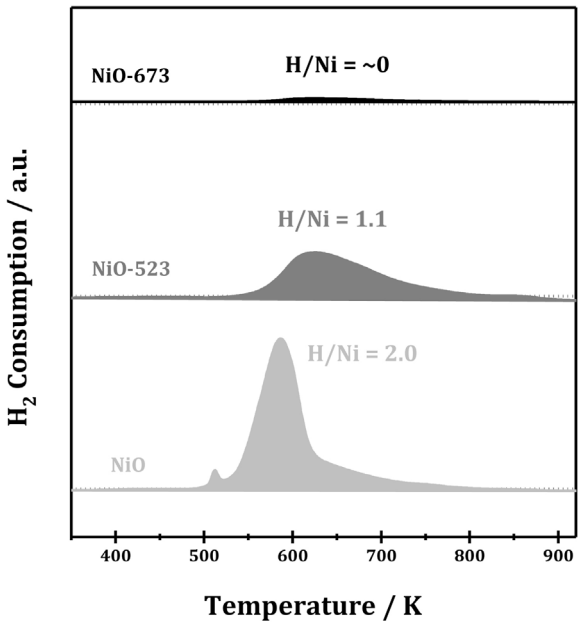


**Fig. 2.** $H_2$-TPR profiles of NiO, NiO-523 and NiO-673 samples.

## 3. Results and discussions

### 3.1. Formation of heterostructured Ni/NiO composite

Fig. 1 depicts the in situ XRD patterns of NiO samples, which are conducted at different reduction temperatures in hydrogen stream. XRD pattern of the as-prepared NiO sample confirms the phase purity of nickel oxide (JCPDS-47-1049) [69]. When NiO sample is treated in hydrogen at 473 K (NiO-473), the dominating phase of sample is still nickel oxide. However, very weak peaks corresponding to the (111) and (200) diffractions of metallic nickel (JCPDS-04-0850) could be detected, indicating the formation of trace metallic nickel species by hydrogen reduction at 473 K [70]. With reduction temperature increased to 523 K (NiO-523), the (111), (200) and (220) diffractions of metallic nickel become more distinct, and nickel oxide phase still existed. Obviously, NiO-523 exists as a mixture of metallic nickel and nickel oxide. In contrast, with the reduction temperature further increased to 573 and 673 K (NiO-573 and NiO-673), metallic nickel appears as the excluded phase and no signs of nickel oxide can be observed in the XRD patterns. On the basis of the in situ XRD patterns, the gradually reduction of nickel oxide (NiO: JCPDS-47-1049) to metallic nickel (Ni: JCPDS-04-0850) is clearly demonstrated.

For a better understanding of the reduction process of nickel oxide, $H_2$-TPR profiles of NiO, NiO-523 and NiO-673 samples are shown in Fig. 2. For NiO, hydrogen consumption peaks in the temperature range of 473–773 K with H/Ni ratio of 2.0 are observed, corresponding to the reduction of NiO to metallic nickel. For NiO-673, no hydrogen consumption can be observed, revealing the exclusive existence of metallic nickel in the sample. While for NiO-523, a relatively broad hydrogen consumption peak in the temperature range of 523–773 K is observed. The H/Ni ratio is calculated to be 1.1, indicating the existence of near equal quantities of metallic nickel and nickel oxide. That is, NiO-523 is a composite of Ni/NiO.

The surface states of nickel catalysts were analyzed by in situ XPS and the results are shown in Fig. 3. In the Ni 2p region, four characteristic features, i.e. $Ni^{2+}$ $2p_{3/2}$ main peak and its satellite at ~854 and ~862 eV, respectively, as well as $Ni^{2+}$ $2p_{1/2}$ main peak and

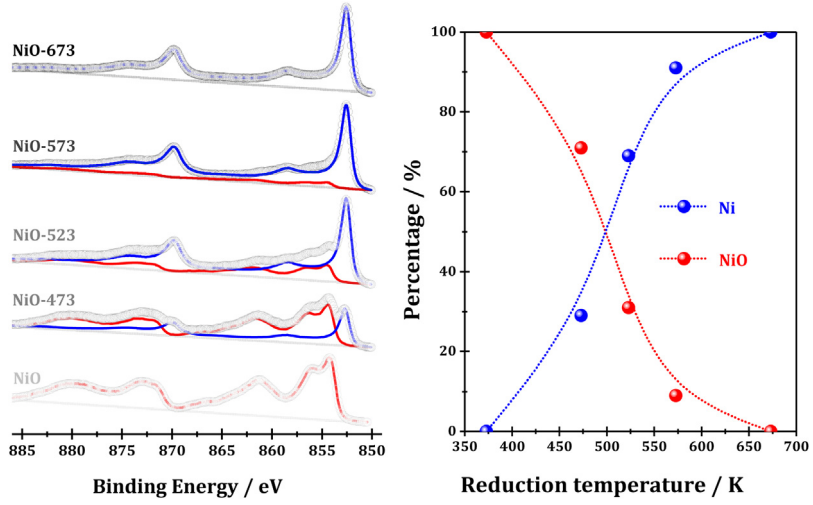


**Fig. 3.** In situ Ni 2p XPS of nickel oxide during hydrogen treatment (left chart) and the surface composition obtained from XPS (right chart).

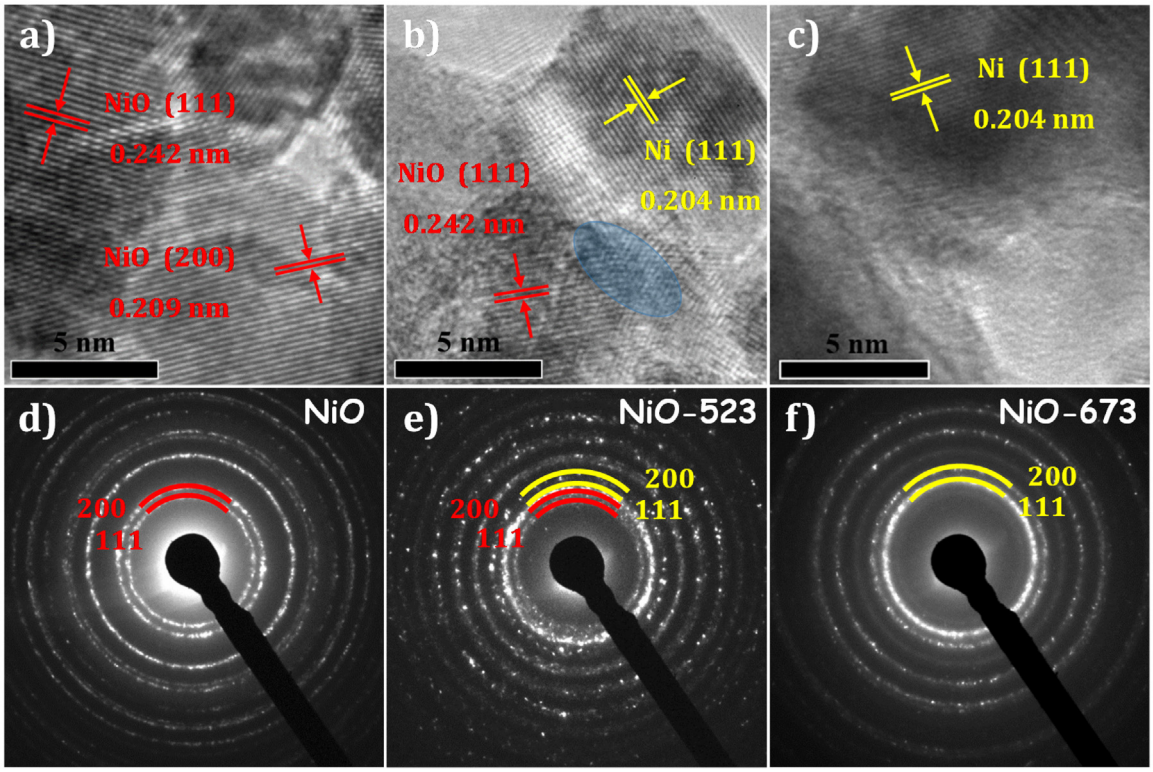


**Fig. 4.** HRTEM images and corresponding SAED patterns of NiO, NiO-523 and NiO-673 samples.

its satellite at ~872 and ~879 eV, respectively, are observed for NiO (Fig. 3, left chart), which are in good accordance with the previous reports [71,72] and match perfectly well with standard NiO (red line). For NiO-673, binding energy values at ~852 and ~870 eV are observed, corresponding to $Ni^0$ $2p_{3/2}$ and $2p_{1/2}$, respectively. The spectrum of NiO-673 matches well with standard metallic Ni (blue line), confirming metallic nickel as the exclusive surface species in NiO-673. While for NiO-473 and Ni-523, spectral features corresponding to both $Ni^{2+}$ (~854, ~862, ~872 and ~879 eV; red line) and $Ni^0$ (~852 and ~870 eV; blue line) can be observed, indicating the existence of both NiO and metallic Ni in these two samples [73]. For NiO-573, $Ni^0$ is the dominating species (~852 and ~870 eV; blue line), and trace $Ni^{2+}$ can also be identified (~854, ~862, ~872 and ~879 eV; red line), as clearly shown in the enlarged view of Ni 2p XPS (Fig. S1). According to the in situ XPS results, a gradual reduction of surface nickel oxide to metallic nickel is confirmed and the changes in the surface composition with hydrogen treatment temperature are shown in Fig. 3 (right chart). It can be concluded that surface Ni-NiO composite is formed by treating parent NiO in hydrogen at certain temperature, e.g. 473–573 K.

To confirm the surface reduction of nickel oxide, in situ FTIR spectra of CO adsorption on NiO, NiO-523 and NiO-673 were performed (Fig. S2). For parent NiO sample, only bands of gas-phase or physisorbed CO at 2111 $cm^{-1}$ and 2173 $cm^{-1}$ are detected at room temperature [74,75]. Upon hydrogen treatment at 523 K for 1 h (NiO-523), IR band at 2090 $cm^{-1}$ due to carbonyl on metallic nickel appears, indicating the reduction of surface nickel oxide to metallic nickel. This characteristic band becomes stronger with reduction temperature increase to 673 K (NiO-673). The in situ FTIR spectra of CO adsorption reveal the formation of metallic nickel on the surface upon hydrogen treatment at elevated temperatures, supporting the results from in situ XPS analysis (Fig. 3).

Microscopic analysis can provide useful information on the morphology and structure of solid samples, and it is employed in the characterization of nickel catalysts in this study. As shown in high-resolution TEM (HRTEM) in Fig. 4a, the parent NiO sample appears to be stacking of nanometric particles. Well resolved lattice fringes with interplanar distance of 0.242 and 0.209 nm are observed, corresponding to (111) and (200) planes of NiO, respectively [76]. The selected area electron diffraction (SAED) patterns (Fig. 4d) also support the presence of (111) and (200) diffraction rings in NiO. Upon hydrogen treatment at 673 K, NiO-673 appears to be larger nanoparticles of a dozen of nanometers, and the interplanar distance of lattice fringe is determined to be 0.203 nm (Fig. 4c), corresponding to (111) planes of metallic nickel [77]. The exclusive existence of metallic nickel phase is verified by SAED patterns (Fig. 4f), where diffraction rings corresponding to Ni (111) and (200) can be clearly observed. While for NiO treated in hydrogen at 523 K, i.e. NiO-523, both NiO (111) (interplanar distance of 0.242 nm) and Ni (111) (interplanar distance of 0.204 nm) can be identified (Fig. 4b), also confirmed by the SAED patterns (Fig. 4e). These observations are in good agreement with characterization results from XRD (Fig. 1), $H_2$-TPR (Fig. 2) and XPS (Fig. 3). Besides, the formation of Ni-NiO heterojunctions, as marked in the HRTEM image, can be observed, which might result in a cooperation effects in catalysis (vide infra).

### 3.2. Levulinic acid hydrogenation to GVL catalyzed by Ni/NiO

The hydrogenation of levulinic acid to GVL were performed in a high-pressure batch reactor and the catalytic performance of various heterogeneous nickel catalysts are summarized in Table 1 (time-dependent catalytic behaviors shown in Fig. S3). From **Entry 1**, we can see that NiO is a selective but not a very active catalyst for the hydrogenation of levulinic acid to GVL with a low mass activity of 0.8 mmol/h/g, in consistent with previous reports [30]. We find, by accident, that treatment in hydrogen at elevated temperature can significant promote the activity of parent NiO. Typically, an eight times higher mass activity (6.7 mmol/h/g, **Entry 2**) is achieved with NiO-473. If the hydrogen treatment tempera-

**Table 1**
Hydrogenation of levulinic acid to GVL over various nickel catalysts.[a]

| Entry | Catalyst | $S_{BET}$ [$m^2$/g] | Surface Phase | Mass activity [mmol/h/g] | Specific activity [μmol/h/$m^2$] | Selectivity [%][b] |
|---|---|---|---|---|---|---|
| **1** | NiO | 98 | NiO | 0.8 | 8 | >99.9 |
| **2** | NiO-473 | 56 | NiO & Ni | 6.7 | 120 | >99.9 |
| **3** | NiO-523 | 20 | NiO & Ni | 14.1 | 705 | >99.9 |
| **4** | NiO−523[c] | 21 | NiO & Ni | 14.3 | 681 | >99.9 |
| **5** | NiO-573 | 19 | NiO & Ni | 11.5 | 605 | >99.9 |
| **6** | NiO-673 | 19 | Ni | 1.3 | 68 | >99.9 |
| **7** | NiO-773 | 18 | Ni | 1.2 | 65 | >99.9 |
| **8** | Nickel foil[d] | 5 | Ni | 0.3 | 60 | >99.9 |
| **9** | NiO + NiO-673 | 57 | NiO & Ni | 1.0 | 17 | >99.9 |
| **10** | 20%Ni/$SiO_2$[e] | 180 | Ni | 0.8 | 4 | >99.9 |
| **11** | 20%Ni/$ZrO_2$[e] | 58 | Ni | 0.3 | 5 | >99.9 |

[a] Reaction conditions: 0.2 g catalyst, 10 mmol levulinic acid, 100 mL dioxane, T = 393 K, 2 MPa $H_2$.
[b] at levulinic acid conversion of ~10%.
[c] Repeating experiment.
[d] Sigma-Aldrich, thickness 0.125 mm, >99.9%.
[e] Prepared by wet-impregnation, followed by reduction at 673 K.

ture is increased to 523 K, an eighteen times higher mass activity is achieved (14.1 mmol/h/g, **Entry 3**). Further increase in hydrogen treatment temperature to 573 K results in a noticeable decrease in the mass activity (11.5 mmol/h/g, **Entry 5**). Higher treatment temperature of 673 or 773 K results in a sharp decrease in the activity, and low mass activity of 1.3 and 1.2 mmol/h/g is achieved with NiO-673 and Ni-773 (**Entry 6 & 7**), respectively. It is known that the high temperature treatments may bring about significant decreases in the surface area, which accordingly shows great impacts on the mass activity of catalysts. Herein, the surface area of nickel catalysts is measured by low temperature nitrogen adsorption/desorption and a gradual decrease surface area from 56 to 18 $m^2$/g with increasing hydrogen treatment temperature from 473 to 673 K is observed. With the measured surface area values, we can calculate the specific activity to illustrate the intrinsic characters of catalysts in the reaction. As shown in Table 1, the specific activity of NiO dramatically increases by fifteen times, i.e. from 8 to 120 μmol/h/$m^2$, upon hydrogen treatment at 473 K. The highest specific activity of 705 μmol/h/$m^2$ is achieved with NiO-523, which is almost two orders of magnitude higher than parent NiO. Integrating the activity data in Table 1 and XPS results in Fig. 3, we propose that co-existence of surface NiO and Ni species in catalysts is essential for their remarkable specific activity. If nickel oxide is fully reduced to Ni, i.e. only surface Ni species are present, the specific activity of catalysts decreases significantly to the level of 60–68 μmol/h/$m^2$ (**Entry 6–8**). On the other hand, the physical mixture of NiO and NiO-673 is employed as catalyst in the reaction and a very low specific activity of 17 μmol/h/$m^2$ is achieved (**Entry 9**). Ni/$SiO_2$ and Ni/$ZrO_2$ prepared by wet-impregnation also exhibited very low activity (**Entry 10 & 11**). Obviously, the cooperation of surface NiO and Ni species is required for the high activity in levulinic acid hydrogenation to GVL. In this context, the formation of heterojunctions, which has been frequently reported for semiconductor photocatalysts [78], should be an ideal choice, as revealed by TEM analysis (Fig. 4b). On the basis of primary activity data (Table 1) and spectral characterization results (Figs. 3 and 4), we come to the conclusion that the cooperation of surface NiO and Ni species should be an efficient strategy to promoting the activity of nickel catalysts in levulinic acid hydrogenation to GVL. The ratio of Ni/NiO can influence the catalytic activity of nickel catalysts to a great extent. Currently, we are not able relate the specific activity with Ni/NiO ratio due to the lack of information on real surface Ni/NiO ratio (XRD and TPR analysis give the bulk information while XPS analysis gives sub–10 nm depth surface information), nevertheless, NiO-523 can be experimentally optimized among several samples investigated. It should be mentioned that the preparation parameters, e.g. nickel precursor (Fig. S4), precipitator, hydrogen concentration for partial reduction (Fig. S5) and reduction duration (Fig. S6), might influence the catalytic performance of nickel catalysts. With the precise control of these parameters, the quality of nickel catalysts can be well controlled, as illustrated by results from repeating experiment (**Entry 4**). Besides, the hydrogen pressures in the reaction system can also influence the catalytic performance of nickel catalysts (Fig. S7) and the catalytic data shown in this work have been optimized.

For a better understanding of the catalytic properties of nickel catalysts, three representative catalysts, i.e. NiO with exclusive surface NiO species, NiO-523 with co-existence of surface Ni-NiO species and NiO-673 with exclusive surface Ni species, are selected for further studies. The kinetic plots of levulinic acid to GVL conversion over these three catalysts are shown in Fig. 5. In all catalytic tests included, a linear increase in the GVL yield with prolonged reaction time is achieved at GVL yields below 80%, indicating the apparent zero-order reaction with respect to levulinic acid under our experimental conditions (excess hydrogen). Besides, the reaction rates of levulinic acid hydrogenation to GVL over all nickel catalysts are not influenced by the initial levulinic acid dosage (Fig. S8), excluding the effects of levulinic acid concentration on the reaction rate. NiO with exclusive surface NiO species exhibits poor catalytic activity at the reaction temperature below 413 K (Fig. 5a), while considerable catalytic activity is achieved with the same catalyst at the reaction over 423 K (Fig. 5b). It seems that there is a sudden change of activity within temperature range of 413–423 K, which might be due to the in situ surface reduction of catalyst (vide infra). NiO-523 with the co-existence of surface Ni-NiO species exhibits much higher activity than parent NiO with exclusive surface NiO species under identical reaction conditions (Fig. 5b). In fact, the catalytic activity of NiO-523, i.e. Ni/NiO heterojunction, is comparable with the best results from non-precious-metal catalysts under similar reaction conditions (see Table S1 for details). The remarkable catalytic activity and recyclability (vide infra) as well as the low-cost property make Ni/NiO heterojunction an attracting catalyst for potential application in levulinic acid hydrogenation to GVL. NiO-523 can efficiently catalyze the hydrogenation of levulinic acid to GVL at 373 K and under 2 MPa hydrogen, mild conditions commonly employed for homogeneous catalysis system [79]. With prolonged reaction time to 24 h, the complete conversion of levulinic acid to GVL (>99.9% GVL yield) can be achieved (Fig. S9). NiO-673 with exclusive surface Ni species exhibits very low activity in the temperature range of 383–413 K, and increasing reaction temperature does not bring about a sudden change in the activity as that observed for NiO (Fig. S10).

The Arrhenius plots of reaction rate over representative nickel catalysts are performed, and the apparent activation energy values

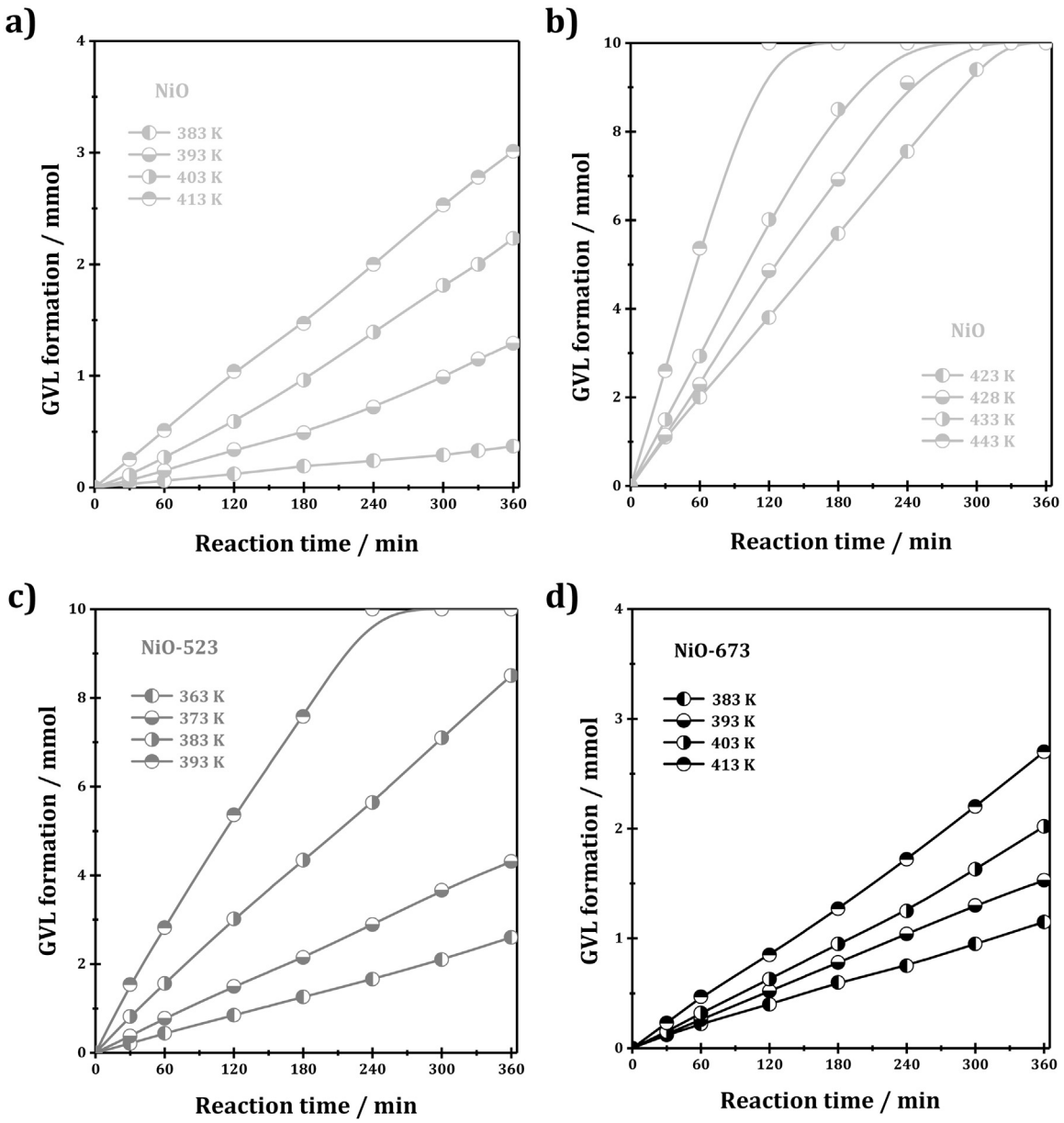


**Fig. 5.** Time-dependent GVL yield over NiO, NiO-523 and NiO-673 catalysts. Reaction conditions: 0.2 g catalyst, 10 mmol levulinic acid, 100 mL dioxane, 2 MPa $H_2$.

for levulinic acid hydrogenation are calculated and shown in Fig. 6. For NiO, two different apparent activation energy values of 93.7 and 67.6 kJ/mol are obtained in the temperature ranges of 383–413 K and 423–443 K, respectively (Fig. 6a & b). The segmented Arrhenius plots are similar to those observed in the case of water-gas shift reaction catalyzed by cobalt catalysts [80]. It means that different catalytic active sites operate in the temperature range of 383–413 and 423–443 K (the impacts from intramolecular esterification of 4-hydroxypentanoic acid to GVL could be excluded in the temperature range of 383–443 K [81]). Tomishige et al. reported that in situ reduction pretreatment for Ir-ReOx/$SiO_2$ catalyst was necessary to achieve high activity in crotonaldehyde hydrogenation, due to the formation of metallic Ir and ReOx through hydrogen treatment [82]. Here, the in situ reduction process should occur on NiO at temperature of >423 K in the liquid phase in the presence of high pressure hydrogen. In order to confirm this process, NiO catalyst after levulinic acid hydrogenation at 433 K for 6 h was recycled and reused at 393 K. As shown in Fig. S11, a three times higher mass activity (2.7 mmol/h/g) compared to the parent NiO (0.8 mmol/h/g) is achieved. These observations clearly demonstrate the active site reconstruction during levulinic acid hydrogenation at 433 K, i.e. in situ surface reduction process.

For NiO-523, the apparent activation energy is calculated to be 70.1 kJ/mol (Fig. 6c), very close to the value of 67.6 kJ/mol from NiO in the temperature range 383–413 K. It can be expected that the same type of catalytic active sites operate in NiO-523 and NiO (383–413 K), i.e. Ni/NiO heterojunctions. That is, the in situ surface reduction of NiO to Ni/NiO takes place during levulinic acid hydrogenation at >423 K. Moreover, the in situ surface reduction should be a very fast process, which does not result in an observable changes in the linear kinetic behaviors (Fig. 5b).

While for NiO-673 with exclusive surface Ni species, an apparent activation energy value of 33.2 kJ/mol is obtained (Fig. 6d), significantly lower than those calculated from NiO and NiO-523. However, the low activation energy value of NiO-673 does not lead to a high catalytic activity in levulinic acid hydrogenation (Fig. 5d) due to the very low apparent pre-exponential factor of $2.7*10^4$ mmol/h/g.

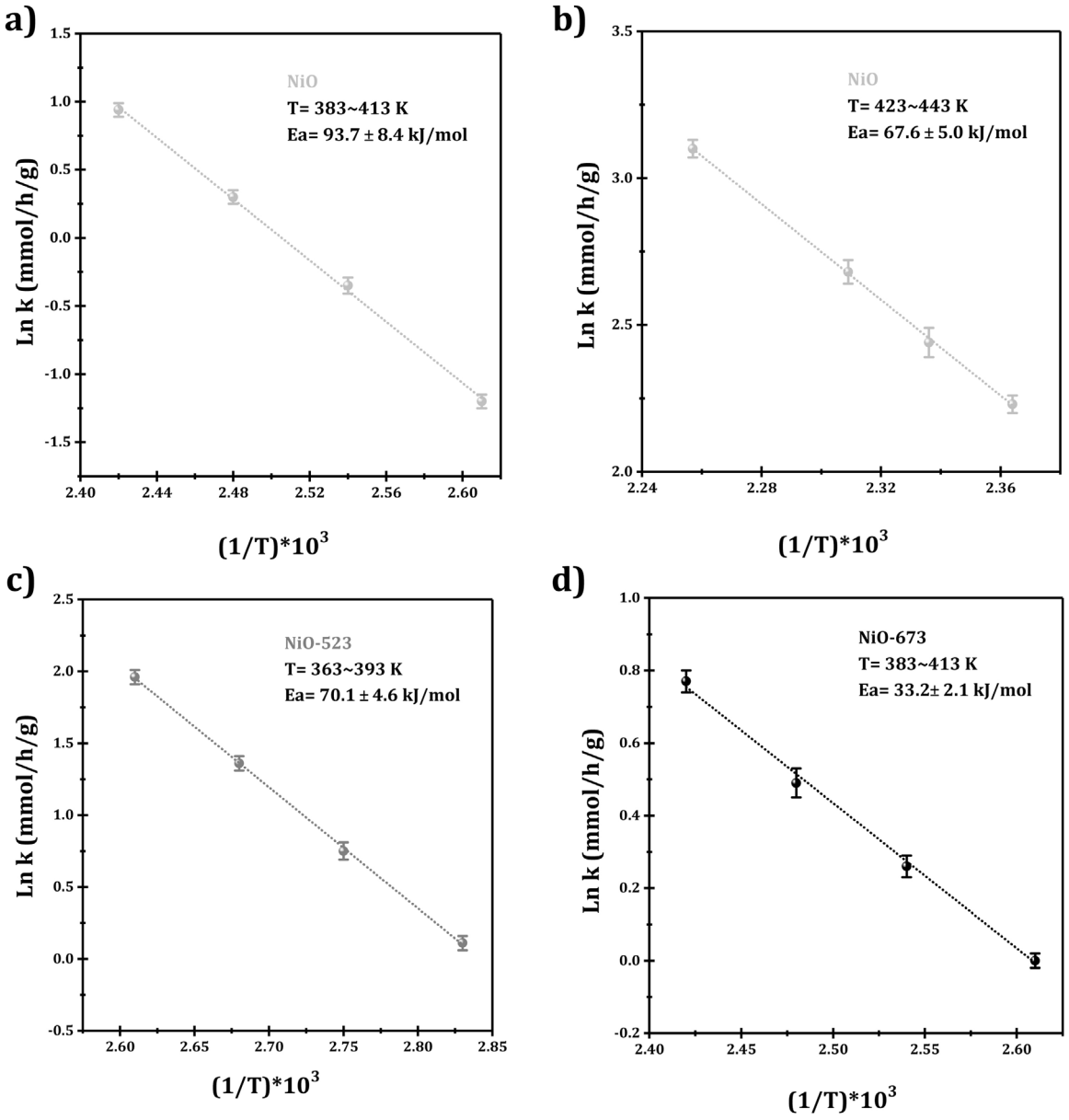


**Fig. 6.** Arrhenius plots of levulinic acid hydrogenation to GVL over NiO (a, b), NiO-523 (c) and NiO-673 (d) catalysts.

### 3.3. Catalytic stability of Ni/NiO heterojunctions

To verify the heterogeneous behavior of Ni/NiO composite, a catalyst removal test was performed. As shown in Fig. 7, the reaction stops immediately after catalyst removal through filtration and the GVL keeps nearly unchanged in the subsequent hours. Meanwhile, no leaching of nickel species in the liquid phase can be detected by ICP analysis (<0.5 ppm). All these experimental observations confirm the heterogeneous nature of heterostructured Ni/NiO composite in levulinic acid hydrogenation to GVL.

Catalytic stability is a big problem for practical liquid-phase hydrogenation of levulinic acid, especially in polar solvent. Supported ruthenium catalysts are very active in levulinic acid hydrogenation, however, only $Ru/ZrO_2$ exhibits good stability in the reaction [83]. A significant deactivation could be observed already in the first recycle of commercial benchmark catalyst Ru/C [84]. For NiO-523 with the co-existence of NiO and Ni surface species, the catalytic stability might be a more difficult task to accomplish. To our surprise, NiO-523 exhibits outstanding stability in the reaction and it can be recycled (through simple centrifugation and washing) for 10 times without a noticeable loss of activity (Fig. 8). Obviously, the surface composition of Ni-NiO is stable under our reaction conditions. In a whole, the remarkable catalytic activity, the perfect stability as well as the low-cost property of heterostructured Ni/NiO composite make it a promising catalyst for large-scale production of GVL from levulinic acid hydrogenation.

### 3.4. Theoretical calculations of reactant adsorption on Ni and NiO surfaces

Theoretical calculations are very helpful in explaining the mechanism of levulinic acid hydrogenation [85,86], and here primary first principle calculations are performed to improve our understanding of the cooperation of Ni-NiO in the reaction. The adsorption of H, $H_2$ and levulinic acid on pure metallic Ni and NiO was calculated separately. According to TEM observations, two surface models of Ni (111) and NiO (111) were constructed to represent the metallic Ni and NiO catalysts, respectively. Details of

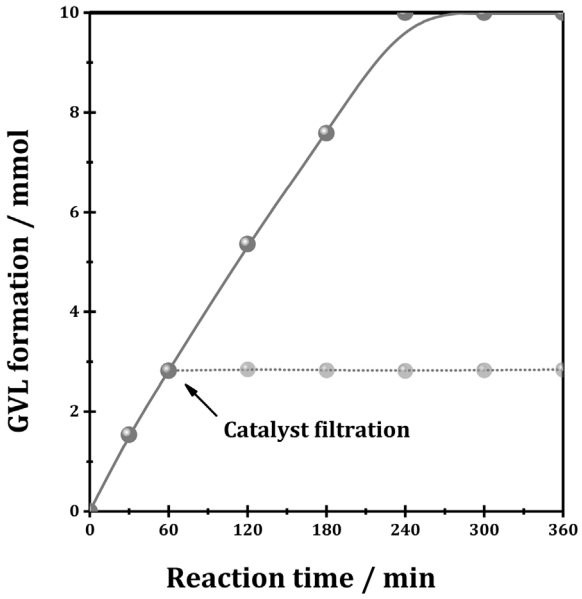


**Fig. 7.** Levulinic acid hydrogenation to GVL catalyzed by NiO-523 with or without the removal of catalyst after reaction for 1 h. Reaction conditions: 0.2 g NiO-523, 10 mmol levulinic acid, 100 mL dioxane, T = 393 K, 2 MPa $H_2$.

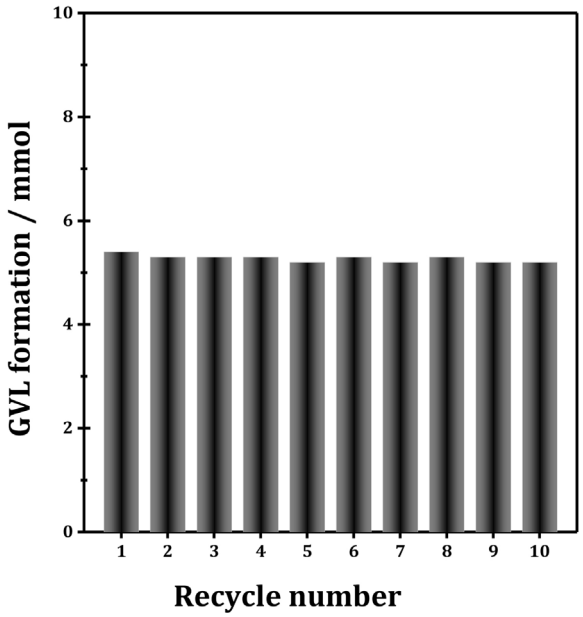


**Fig. 8.** Recycling test in levulinic acid hydrogenation to GVL over NiO-523 catalyst. Reaction conditions: 0.2 g NiO-523, 10 mmol levulinic acid, 100 mL dioxane, T = 393 K, reaction time = 2 h, 2 MPa $H_2$.

**Table 2**
Absorption energy (eV) of H, $H_2$, levulinic acid on Ni (111) and NiO (111), with corresponding bond length.

| Substrate | Surface | $E_{ads}$ (eV) | Bond length (Å) |
|---|---|---|---|
| $H_2$ | P (2 × 2) Ni (111) | −0.29 | H—Ni: 1.60 |
| | P (2 × 2) NiO (111) | −0.10 | H—O: 2.67 |
| H | P (2 × 2) Ni (111) | −2.80 | H—Ni: 1.70 |
| | P (2 × 2) NiO (111) | −2.58 | O—Ni: 0.97 |
| Levulinic acid | P (4 × 4) Ni (111) | −0.40 | O—Ni: 2.01 |
| | P (4 × 4) NiO (111) | −2.90 | O—Ni: 2.06 |

the lowest energy structures of H, $H_2$ and levulinic acid adsorbed on Ni (111) and NiO (111) are illustrated in Fig. 9 and the corresponding data summarized in Table 2. For H and $H_2$ adsorbed on Ni (111) and NiO (111), the bond length is the minimum length between adsorbed chemical species and the catalyst surface atoms. The adsorption energy values of H on Ni (111) and NiO (111) are −2.80 and −2.58 eV, respectively, in good agreement with previous reports [87–89]. $H_2$ adsorption energy values on the Ni (111) and NiO (11) are −0.29 and −0.10 eV, respectively. These results reveal that $H_2$ prefers to adsorb on the Ni (111) over NiO (111) followed by dissociation into atomic hydrogen. As for levulinic acid adsorption, the bond length is the distance between oxygen atom of carbonyl group and surface atoms. A very strong interaction between levulinic acid and NiO (111) is obtained with an adsorption energy value of −2.90 eV. In contrast, the levulinic acid adsorption energy value on Ni (111) is only −0.40 eV. Clearly, levulinic acid prefers to adsorb on NiO (111) over Ni (111).

The unique catalytic performance of Ni/NiO can be well explained by the results from theoretical calculations. On NiO (111), levulinic acid strongly adsorbs on the surface and then covers the surface, making the surface not available for $H_2$ adsorption and

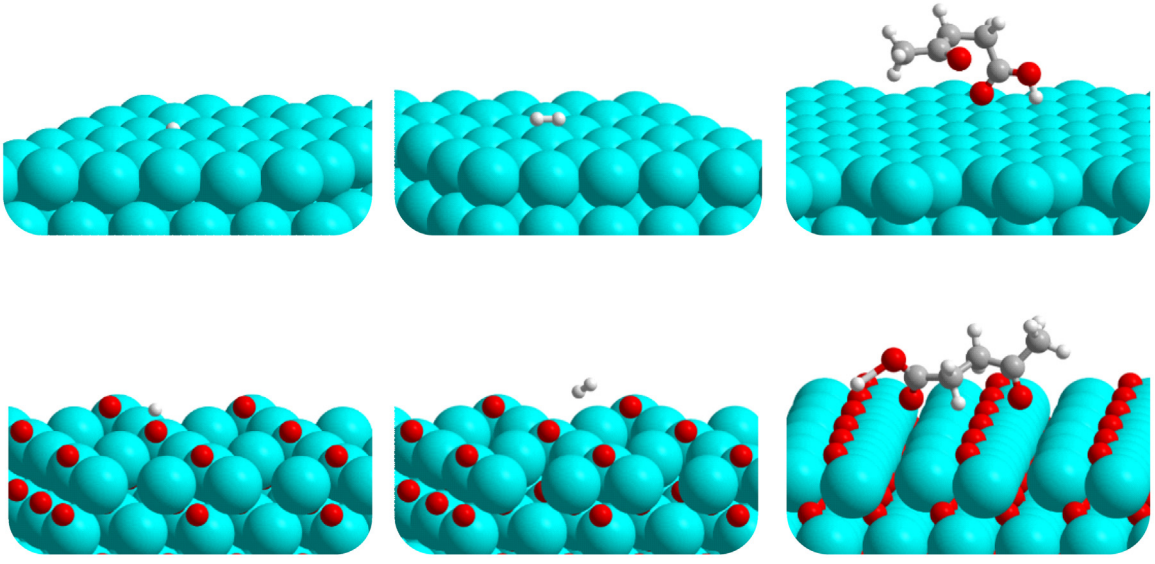

**Fig. 9.** Structure models for H, $H_2$ and levulinic acid adsorption on Ni (111) and NiO (111).

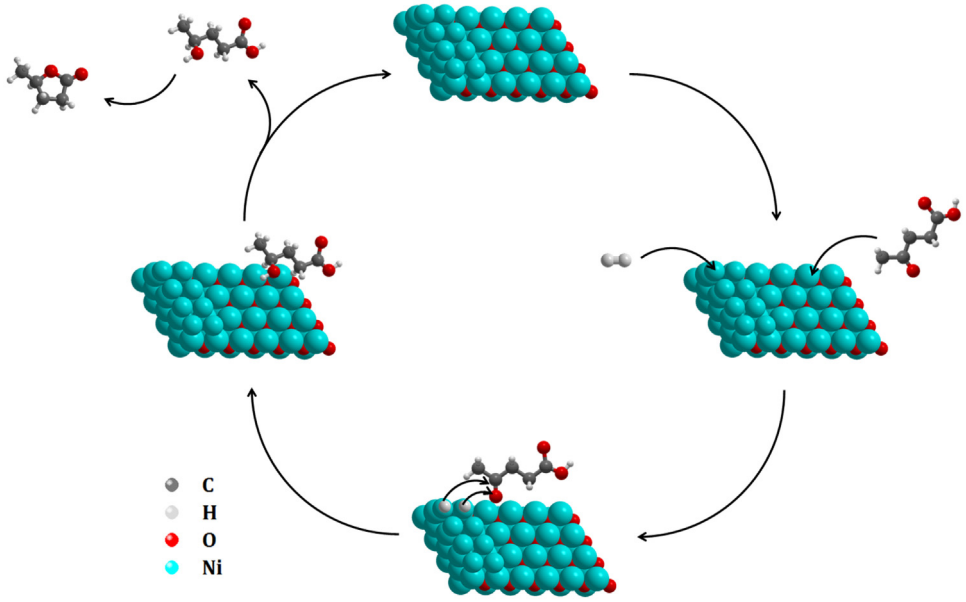


**Fig. 10.** Proposed mechanism for hydrogenation of levulinic acid to GVL on Ni/NiO.

subsequent dissociation. Therefore, the reaction between adsorbed levulinic acid with gaseous hydrogen should be a feasible pathway for levulinic acid hydrogenation, which undergoes a high apparent activation energy value of 93.7 kJ/mol. On Ni (111), the competing adsorption of $H_2$ and levulinic acid may take place due to the similar adsorption energy values (0.29 versus 0.40 eV, Table 2). This competition will result in the lack of effective active sites for levulinic acid hydrogenation (two adsorbed species in adjacent sites are required), as reflected by the low apparent pre-exponential factor of $2.7*10^4$ mmol/h/g.

If both surface Ni (111) and NiO (111) are available in the catalyst (Fig. 4b), the hydrogenation of levulinic acid can undergo a cooperative reaction pathway. As shown in Fig. 10, $H_2$ preferentially adsorbs on Ni (111) with an energy value of 0.29 eV, followed by an exothermic dissociation into atomic hydrogen. Meanwhile, levulinic acid preferentially adsorbs on NiO (111) with an energy value of −2.90 eV. The adsorbed levulinic acid on NiO (111) can react with adsorbed H on Ni (111) in the neighboring regions to produce 4-hydroxy-pentanoic acid via Langmuir-Hinshelwood mechanism. In this context, the formation of Ni/NiO heterojunctions, as observed in NiO-523, is mostly desirable. Since different active sites are involved in levulinic acid hydrogenation over Ni/NiO, the apparent zero order kinetics with respect to levulinic acid (Fig. 5) does not conflict with the proposed Langmuir-Hinshelwood mechanism. Unfortunately, we fail to construct the surface model of Ni/NiO due to its intrinsic complexity and instability and, therefore, a detailed reaction pathway study is not available. Nevertheless, the primary calculation results, together with experimental observations, can well explain the cooperation of Ni/NiO in levulinic acid hydrogenation.

## 4. Conclusion

Heterogeneous catalytic hydrogenations are important reactions with industrial relevance, and non-precious metal hydrogenation catalysts with adequate performance are being pursued. Herein, with levulinic acid hydrogenation to γ-valerolactone as a model reaction, we show that Ni/NiO heterojunctions from the partial reduction of nickel oxide can efficiently catalyze hydrogenation reactions.

Hydrogen treatment on parent nickel oxide at elevated temperature of 473–573 K leads to the partial reduction of nickel oxide to metallic nickel and the formation of Ni/NiO heterojunctions, as verified by in situ XRD, XPS and TEM analysis. When employed in the catalytic levulinic acid hydrogenation, a remarkable specific activity of 705 μmol/h/$m^2$ is achieved with Ni/NiO heterojunctions, being almost two orders of magnitude higher than parent NiO (8 μmol/h/$m^2$) and over one order of magnitude higher than metallic Ni (60–68 μmol/h/$m^2$) under identical mild reaction conditions, i.e. at 393 K and under 2 MPa $H_2$. In addition to the high activity and perfect selectivity (> 99.9%) in levulinic acid hydrogenation to GVL, good stability and recyclability in the reaction can be achieved with Ni/NiO heterojunctions, making them promising low-cost catalysts for industrial applications.

Kinetic analysis results reveal the different apparent activation energy values of 93.7, 70.1 and 33.2 kJ/mol for NiO, Ni/NiO and metallic Ni, respectively, hinting the different levulinic acid hydrogenation pathways on these catalysts. Theoretical calculations indicate that levulinic acid preferentially adsorbs on NiO surface, while $H_2$ preferentially adsorbs on metallic Ni surface followed by dissociation to atomic hydrogen. A cooperative Langmuir-Hinshelwood mechanism can be proposed for levulinic acid hydrogenation on Ni/NiO heterojunctions. The concept of cooperative catalysis on metal/oxide heterojunctions should be a general strategy for efficient hydrogenations.

## Conflict of interest

The authors declare no competing financial interest.

## Acknowledgements

This work is supported by the National Natural Science Foundation of China (21421001, 21573113) and Municipal Natural Science Foundation of Tianjin (13RCGFGX01124).

## Appendix A. Supplementary data

Supplementary data associated with this article can be found, in the online version, at http://dx.doi.org/10.1016/j.apcatb.2017.05.073.

## References


[1] G.W. Huber, S. Iborra, A. Corma, Chem. Rev. 106 (2006) 4044–4098.
[2] A. Corma, S. Iborra, A. Velty, Chem. Rev. 107 (2007) 2411–2502.
[3] V. Choudhary, A.B. Pinar, S.I. Sandler, D.G. Vlachos, R.F. Lobo, ACS Catal. 1 (2011) 1724–1728.
[4] M.M. Antunes, S. Lima, P. Neves, A.L. Magalhães, E. Fazio, F. Neri, M.T. Pereira, A.F. Silva, C.M. Silva, S.M. Rocha, M. Pilinger, A. Urakawa, A.A. Valente, Appl. Catal. B 182 (2016) 485–503.
[5] C. Sievers, I. Musin, T. Marzialetti, M.B. Valenzuela Olarte, P.K. Agrawal, C.W. Jones, ChemSusChem 2 (2009) 665–671.
[6] A.J. Crisci, M.H. Tucker, M.Y. Lee, S.G. Jang, J.A. Dumesic, S.L. Scott, ACS Catal. 1 (2011) 719–728.
[7] Y.J. Pagan-Torres, T. Wang, J.M.R. Gallo, B.H. Shanks, J.A. Dumesic, ACS Catal. 2 (2012) 930–934.
[8] V. Choudhary, S.H. Mushrif, C. Ho, A. Anderko, V. Nikolakis, N.S. Marinkovic, A.I. Frenkel, S.I. Sandler, D.G. Vlachos, J. Am. Chem. Soc. 135 (2013) 3997–4006.
[9] H. Huang, C.A. Denard, R. Alamillo, A.J. Crisci, Y. Miao, J.A. Dumesic, S.L. Scott, H. Zhao, ACS Catal. 4 (2014) 2165–2168.
[10] S.E. Davis, B.N. Zope, R.J. Davis, Green Chem. 14 (2012) 143–147.
[11] X. Zhang, D. Zhang, Z. Sun, L. Xue, X. Wang, Z. Jiang, Appl. Catal. B 196 (2016) 50–56.
[12] P. Carniti, A. Gervasini, F. Bossola, V.D. Santo, Appl. Catal. B 193 (2016) 93–102.
[13] J. Guo, S. Zhua, Y. Cen, Z. Qin, J. Wang, W. Fan, Appl. Catal. B 200 (2017) 611–619.
[14] S. Van de Vyver, J. Thomas, J. Geboers, S. Keyzer, M. Smet, W. Dehaen, P.A. Jacobs, B.F. Sels, Energy Environ. Sci. 4 (2011) 3601–3610.
[15] L. Bui, H. Luo, W.R. Gunther, Y. Román-Leshkov, Angew. Chem. Int. Ed. 52 (2013) 8022–8025.
[16] S. Song, L. Di, G. Wu, W. Dai, N. Guan, L. Li, Appl. Catal. B 205 (2017) 393–403.
[17] D.L. King, L. Zhang, G. Xia, A.M. Karim, D.J. Heldebrant, X. Wang, T. Peterson, Y. Wang, Appl. Catal. B 99 (2010) 206–213.
[18] S.S. Liu, K.Q. Sun, B.Q. Xu, ACS Catal. 4 (2014) 2226–2230.
[19] M.A. Betiha, H.M. Hassan, E.A. El-Sharkawy, A.M. Al-Sabagh, M.F. Menoufy, H.M. Abdelmoniem, Appl. Catal. B 182 (2016) 15–25.
[20] A. Fukuoka, P.L. Dhepe, Angew. Chem. Int. Ed. 45 (2006) 5161–5163.
[21] D.M. Alonso, S.G. Wettstein, J.A. Dumesic, Green Chem. 15 (2013) 584–595.
[22] G.W. Huber, J.W. Shabaker, J.A. Dumesic, Science 300 (2003) 2075–2077.
[23] L.N. Ding, A.Q. Wang, M.Y. Zheng, T. Zhang, ChemSusChem 3 (2010) 818–821.
[24] G.H. Wang, J. Hilgert, F.H. Richter, F. Wang, H.J. Bongard, B. Spliethoff, C. Weidenthaler, F. Schüth, Nat. Mater. 13 (2014) 293–300.
[25] G.H. Wang, X. Deng, D. Gu, K. Chen, H. Tüysüz, B. Spliethoff, C. Weidenthaler, F. Schüth, Angew. Chem. Int. Ed. 128 (2016) 11267–11271.
[26] E.I. Gürbüz, J.M.R. Gallo, D.M. Alonso, S.G. Wettstein, W.Y. Lim, J.A. Dumesic, Angew. Chem. Int. Ed. 52 (2013) 1270–1274.
[27] D. Wang, S.H. Hakim, D.M. Alonso, J.A. Dumesic, Chem. Commun. 49 (2013) 7040–7042.
[28] L. Du, Q.Y. Bi, Y.M. Liu, Y. Cao, H.Y. He, K.N. Fan, Green Chem. 14 (2012) 935–939.
[29] S. Tanaka, K. Fukuda, T. Asada, (Kao Corp.). Patent No. EP1555261A1, 2005.
[30] L.E. Manzer, Appl. Catal. A 272 (2004) 249–256.
[31] M. Chia, J.A. Dumesic, Chem. Commun. 47 (2011) 12233–12235.
[32] L. Du, L. He, S. Zhao, Y.M. Liu, Y. Cao, H.Y. He, K.N. Fan, Angew. Chem. Int. Ed. 123 (2011) 7961–7965.
[33] D. Ding, J. Wang, J. Xi, X. Liu, G. Lu, Y. Wang, Green Chem. 16 (2014) 3846–3853.
[34] J.M. Nadgeri, N. Hiyoshi, A. Yamaguchi, O. Sato, M. Shirai, Appl. Catal. A 470 (2014) 215–220.
[35] K.I. Shimizu, S. Kanno, K. Kon, Green Chem. 16 (2014) 3899–3903.
[36] Y. Yang, G. Gao, X. Zhang, F. Li, ACS Catal. 4 (2014) 1419–1425.
[37] W. Luo, M. Sankar, A.M. Beale, Q. He, C.J. Kiely, P.C. Bruijnincx, P.C.A. Bruijnincx, B.M. Weckhuysen, Nat. Commun. 6 (2015) 6540.
[38] Q. Xu, X. Li, T. Pan, C. Yu, J. Deng, Q. Guo, Y. Fu, Green Chem. 18 (2016) 1287–1294.
[39] A.S. Piskun, J.E. de Haan, E. Wilbers, H.H. van de Bovenkamp, Z. Tang, H.J. Heeres, ACS Sustain. Chem. Eng. 4 (2016) 2939–2950.
[40] P.P. Upare, J.M. Lee, Y.K. Hwang, D.W. Hwang, J.H. Lee, S.B. Halligudi, J.S. Hwang, J.S. Chang, ChemSusChem 4 (2011) 1749–1752.
[41] A.M. Hengne, C.V. Rode, Green Chem. 14 (2012) 1064–1072.
[42] K. Yan, J. Liao, X. Wu, X. Xie, RSC Adv. 3 (2013) 3853–3856.
[43] K. Hengst, M. Schubert, H.W. Carvalho, C. Lu, W. Kleist, J.D. Grunwaldt, Appl. Catal. A 502 (2015) 18–26.
[44] J. Quiroz, E.F. Mai, V.T. da Silva, Top. Catal. 59 (2016) 148–158.
[45] M.D. Astuti, T. Hara, N. Ichikuni, S. Shimazu, Catal. Sci. Technol. 6 (2016) 2955–2961.
[46] K. Jiang, D. Sheng, Z. Zhang, J. Fu, Z. Hou, X. Lu, Catal. Today 274 (2016) 55–59.
[47] S. Ishikawa, D.R. Jones, S. Iqbal, C. Reece, D.J. Morgan, D.J. Willock, P.J. Miedziak, J.K. Bartley, J.K. Edwards, T. Murayama, W. Ueda, G.J. Hutchings, Green Chem. 19 (2017) 225–236.
[48] J.M. Tukacs, R.V. Jones, F. Darvas, G. Dibó, G. Lezsák, L.T. Mika, RSC Adv. 3 (2013) 16283–16287.
[49] V. Mohan, C. Raghavendra, C.V. Pramod, B.D. Raju, K.S.R. Rao, RSC Adv. 4 (2014) 9660–9668.
[50] V. Mohan, V. Venkateshwarlu, C.V. Pramod, B.D. Raju, K.S.R. Rao, Catal. Sci. Technol. 4 (2014) 1253–1259.
[51] V. Kumar, G. Naresh, M. Sudhakar, C. Anjaneyulu, S.K. Bhargava, J. Tardio, V.K. Reddy, A. Venugopal, RSC Adv. 6 (2016) 9872–9879.
[52] P.P. Upare, Y.K. Hwang, J.M. Lee, D.W. Hwang, J.S. Chang, ChemSusChem 8 (2015) 2345–2357.
[53] Z. Zhang, ChemSusChem 9 (2016) 156–171.
[54] R.V. Jagadeesh, A.E. Surkus, H. Junge, M.M. Pohl, J. Radnik, J. Rabeah, H. Huan, V. Schunemann, A. Brückner, M. Beller, Science 342 (2013) 1073–1076.
[55] F.A. Westerhaus, R.V. Jagadeesh, G. Wienhöfer, M.M. Pohl, J. Radnik, A.E. Surkus, J. Rabeah, K. Junge, H. Junge, M. Nielsen, A. Brückner, M. Beller, Nat. Chem. 5 (2013) 537–543.
[56] S. Pisiewicz, D. Formenti, A.E. Surkus, M.M. Pohl, J. Radnik, K. Junge, C. Topf, S. Bachman, M. Scalone, M. Beller, ChemCatChem 8 (2016) 129–134.
[57] L. Liu, P. Concepción, A. Corma, J. Catal. 340 (2016) 1–9.
[58] H. Zhou, J. Song, H. Fan, B. Zhang, Y. Yang, J. Hu, Q. Zhu, B. Han, Green Chem. 16 (2014) 3870–3875.
[59] G. Kresse, J. Hafner, Phys. Rev. B 47 (1993) 558–561.
[60] G. Kresse, J. Furthmüller, Comput. Mater. Sci. 6 (1996) 15–50.
[61] P.E. Blöchl, Phys. Rev. B 50 (1994) 17953–17979.
[62] J.P. Perdew, K. Burke, M. Ernzerhof, Phys. Rev. Lett. 77 (1996) 3865–3868.
[63] S.L. Dudarev, G.A. Botton, S.Y. Savrasov, C.J. Humphreys, A.P. Sutton, Phys. Rev. B 57 (1998) 1505–1509.
[64] A. Rohrbach, J. Hafner, G. Kresse, Phys. Rev. B 69 (2004) 075413.
[65] A. Rohrbach, J. Hafner, Phys. Rev. B 71 (2005) 045405.
[66] F. Cinquini, L. Giordano, G. Pacchioni, A.M. Ferrari, C. Pisani, C. Roetti, Phys. Rev. B 74 (2006) 165403.
[67] D. Wolf, Phys. Rev. Lett. 68 (1992) 3315–3318.
[68] A. Barbier, C. Mocuta, H. Kuhlenbeck, K.F. Peters, B. Richter, G. Renaud, Phys. Rev. Lett. 84 (2000) 2897–2900.
[69] Y. Zhao, B. Zhao, J. Liu, G. Chen, R. Gao, S. Yao, M. Li, Q. Zhang, L. Gu, J. Xie, X. Wen, L.Z. Wu, C.H. Tung, D. Ma, T. Zhang, Angew. Chem., Int. Ed. 55 (2016) 4215–4219.
[70] J.T. Richardson, R. Scates, M.V. Twigg, Appl. Catal. A 246 (2003) 137–150.
[71] S.C. Petitto, E.M. Marsh, M.A. Langell, J. Phys. Chem. B 110 (2006) 1309–1318.
[72] M.A. Peck, M.A. Langell, Chem. Mater. 24 (2012) 4483–4490.
[73] M. Gong, W. Zhou, M.C. Tsai, J. Zhou, M. Guan, M.C. Lin, B. Zhang, Y. Hu, D.Y. Wang, J. Yang, S.J. Pennycook, B.J. Hwang, H. Dai, Nat. Commun. 5 (2014) 1–6.
[74] E. Escalona Platero, S. Coluccia, A. Zecchina, Langmuir 1 (1985) 407–414.
[75] B. Zhao, X.K. Ke, J.H. Bao, C.L. Wang, L. Dong, Y.W. Chen, H.L. Chen, J. Phys. Chem. C 113 (2009) 14440–14447.
[76] B. Varghese, M.V. Reddy, Z. Yanwu, C.S. Lit, T.C. Hoong, G.V. Subba Rao, B.V.R. Chowadri, A.T.S. Wee, C.T. Lim, C.H. Sow, Chem. Mater. 20 (2008) 3360–3367.
[77] H. Lai, Q. Wu, J. Zhao, L. Shang, H. Li, R. Che, Z. Lyu, J. Xiong, L. Yang, X. Wang, Z. Hu, Energy Environ. Sci. 9 (2016) 2053–2060.
[78] H. Wang, L. Zhang, Z. Chen, J. Hu, S. Li, Z. Wang, J. Liu, X. Wang, Chem. Soc. Rev. 43 (2014) 5234–5244.
[79] F. Liguori, C. Moreno-Marrodan, P. Barbaro, ACS Catal. 5 (2015) 1882–1894.
[80] S. Zhang, J.J. Shan, Y. Zhu, A.I. Frenkel, A. Patlolla, W. Huang, S.J. Yoon, L. Wang, H. Yoshida, S. Takeda, F. Tao, J. Am. Chem. Soc. 135 (2013) 8283–8293.
[81] O.A. Abdelrahman, A. Heyden, J.Q. Bond, ACS Catal. 4 (2014) 1171–1181.
[82] M. Tamura, K. Tokonami, Y. Nakagawa, K. Tomishige, ACS Catal. 6 (2016) 3600–3609.
[83] J. Ftouni, A. Muñoz-Murillo, A. Goryachev, J.P. Hofmann, E.J. Hensen, L. Lu, C.J. Kiely, P.C.A. Bruijnincx, B.M. Weckhuysen, ACS Catal. 6 (2016) 5462–5472.
[84] Z. Yan, L. Lin, S. Liu, Energy Fuels 23 (2009) 3853–3858.
[85] C. Michel, J. Zaffran, A.M. Ruppert, J. Matras-Michalska, M. Jędrzejczyk, J. Grams, P. Sautet, Chem. Commun. 50 (2014) 12450–12453.
[86] O. Mamun, E. Walker, M. Faheem, J.Q. Bond, A. Heyden, ACS Catal. 6 (2016) 215–228.
[87] G. Kresse, J. Hafner, Surf. Sci. 459 (2000) 287–302.
[88] S.G. Wang, D.B. Cao, Y.W. Li, J.G. Wang, H.J. Jiao, J. Phys. Chem. B 110 (2006) 9976–9983.
[89] A. Mohsenzadeh, K. Bolton, T. Richards, Surf. Sci. 627 (2014) 1–10.